



Assessing shallow landslide hazards using the TRIGRS and SHALSTAB models, Serra do Mar, Brazil

Bianca Carvalho Vieira¹ · Nelson Ferreira Fernandes² · Oswaldo Augusto Filho³ · Tiago Damas Martins⁴ · David R. Montgomery⁵

Received: 31 October 2017 / Accepted: 19 March 2018 / Published online: 27 March 2018
© Springer-Verlag GmbH Germany, part of Springer Nature 2018

Abstract

The hillslopes of the Serra do Mar, a system of escarpments and mountains that extend more than 1500 km along the southern and southeastern Brazilian coast, are regularly affected by heavy rainfall that generates widespread mass movements, causing large numbers of casualties and economic losses. This paper evaluates the efficiency of susceptibility mapping for shallow translational landslides in one basin in the Serra do Mar, using the physically based landslide susceptibility models SHALSTAB and TRIGRS. Two groups of scenarios were simulated using different geotechnical and hydrological soil parameters, and for each group of scenarios (A and B), three subgroups were created using soil thickness values of 1, 2, and 3 m. Simulation results were compared to the locations of 356 landslide scars from the 1985 event. The susceptibility maps for scenarios A1, A2, and A3 were similar between the models regarding the spatial distribution of susceptibility classes. Changes in soil cohesion and specific weight parameters caused changes in the area of predicted instability in the B scenarios. Both models were effective in predicting areas susceptible to shallow landslides through comparison of areas predicted to be unstable and locations of mapped landslides. Such models can be used to reduce costs or to define potentially unstable areas in regions like the Serra do Mar where field data are costly and difficult to obtain.

Keywords Mathematical models · Susceptibility mapping · Shallow landslides · Geotechnical and hydrological parameters · Serra do Mar

Introduction

A variety of methods and approaches have been developed and applied in predicting landslide hazards. Physically based mathematical models are considered to be the most objective, due to the direct application of equations that describe

physically relevant processes, and disregard researchers subjective opinions. Such models also can be used to predict landslide susceptibility under different land use scenarios, (Dietrich and Montgomery 1998; Guzzetti et al. 1999; Montgomery and Dietrich 1994; van WESTEN 2004).

✉ Bianca Carvalho Vieira
biancacv@usp.br
Nelson Ferreira Fernandes
nelsonff@acd.ufrj.br
Oswaldo Augusto Filho
oafilho@usp.br
Tiago Damas Martins
td.martins@unifesp.br
David R. Montgomery
bigdirt@uw.edu

¹ Department of Geography, University of São Paulo, Avenida Prof. Lineu Prestes 338. Cidade Universitária, São Paulo CEP: 05508-080, Brazil

² Department of Geography, Federal University of Rio de Janeiro, Rio de Janeiro, Ilha do Fundão, RJ CEP: 21945-970, Brazil

³ São Carlos School of Engineering, University of São Paulo, Av. Trabalhador São-carlense, 400, Centro, São Paulo, SP CEP: 13556590, Brazil

⁴ Cities Institute, Federal University of São Paulo, Avenida Jacu-Pessego, 2630, Itaquera, São Paulo, SP CEP: 08260-001, Brazil

⁵ Department of Earth and Space Science, University of Washington, Johnson Hall, Box 351310, Seattle, WA, USA

Physically based models assess shallow landslide susceptibility through the combination of stability and hydrological modeling. The choice of a particular model must reflect the objectives of its application, consideration of the landslide type, the availability of in situ or secondary data, and accessibility for data collection to inform model parameterization. Among them, such as SHALSTAB/shallow landsliding stability model (Dietrich and Montgomery 1998; Montgomery and Dietrich 1994); dSLAM/Distributed physically based slope stability model (Dhakal and Sidle 2003; Wu and Sidle 1995); SINMAP/Stability Index Mapping) (Morrissey et al. 2001; Pack et al. 1998); TRIGRS/Transient Rainfall Infiltration and Grid-Based Regional Slope Stability (Baum et al. 2002; Iverson 2000); and SLIP/Shallow Landslide Instability Prediction (Montrasio and Valentino 2008).

The main advantages of these models are: (a) ability to apply in different areas without high cost to collect input data, (b) direct comparison among results obtained from different areas, (c) they are easily used in a GIS platform, and (d) they provide a good definition of the role topography plays, which is especially in areas where values for soil properties are not available (Dhakal and Sidle 2003; Sidle and Wu 1999).

Physically based mathematical models have a potential to improve our understanding of landslide hazards and to reduce the costs of identifying unstable areas such as the Serra do Mar, where the difficulty of access due to its steep slopes and dense tropical rainforest preclude direct field investigations. Specifically, this paper evaluates two questions: (a) Which of these physically based mathematical models best assess shallow landslide susceptibility in humid tropical environments like Serra do Mar and (b) does the inclusion of additional parameters (such as rainfall event size) improve the assessment of potentially unstable areas? This article aims to assess the efficiency of susceptibility mapping for shallow translational landslides using SHALSTAB and TRIGRS and tested these models in a basin affected by 356 shallow landslides during an intense rainfall event between January 23 and 24, 1985. In particular, we examine whether including dynamic rainfall improves basin-scale hazard mapping assessments.

SHALSTAB and TRIGRS models

SHALSTAB and TRIGRS calculate shallow translational landslide susceptibility at a drainage basin scale, from coupling a hydrological model to a limit equilibrium slope stability model, using topographical and geotechnical data. However, they have some differences in their mathematical structures, mainly regarding the hydrological model: SHALSTAB assumes steady state, whereas TRIGRS incorporates transient rainfall.

SHALSTAB calculates the critical steady-state rainfall necessary to trigger slope instability at any point in a landscape (Dietrich et al. 1993, 1995; Montgomery and Dietrich 1994; Montgomery et al. 1998). The model considers subsurface flow parallel to the surface, and the hydraulic conductivity and soil thickness, which are treated as uniform for the whole basin. The hydrological model assumes that precipitation infiltrates to a lower conductivity layer and follows topographically determined flow paths, allowing the calculation of the spatial pattern of equilibrium soil saturation. This allows prediction of the critical ratio of the steady-state rainfall “ q ” to the soil transmissivity (T) required to cause slope instability (q/T) via:

$$\frac{q}{T} = \frac{\sin \theta}{(a/b)} \left[\frac{C'}{\rho_w g z \cos^2 \theta \tan \phi} + \frac{\rho_s}{\rho_w} \left(1 - \frac{\tan \theta}{\tan \phi} \right) \right] \quad (1)$$

where “ q ” is the critical rain required to initiate failure [m], “ T ” is the soil transmissivity [m^2/day], “ a ” is the upslope contributing area [m^2], “ b ” is the contour length across which flow is accounted for [m], “ C' ” is the soil effective cohesion [Pa], “ θ ” is the slope angle [$^\circ$, degrees], “ ρ_w ” is the density of water [kN/m^3], “ ρ_s ” is soil unit weight [kN/m^3], “ g ” is gravitational acceleration [m/s^2], “ z ” is the soil thickness [m], and “ ϕ ” is the soil friction angle [degrees].

The TRIGRS model couples a hydrological model and a stability model to predict shallow landslides induced by rainfall events by computing transient pore-pressure changes and their effects on the factor of safety (F_s) at different depths (Baum et al. 2002). In TRIGRS, we can define two boundary conditions: (1) the infinite-depth boundary condition, appropriate for areas where the vertical hydraulic conductivity is relatively uniform with depth and (2) the finite-depth boundary condition, which is appropriate where a more permeable superficial layer overlies a less permeable substrate, such as regolith over bedrock (Baum et al. 2002).

$$F_s = \frac{\tan \phi}{\tan \alpha} + \frac{c - \varphi(Z, t) \gamma_w \tan \phi}{\gamma_s Z \sin \alpha \cos \alpha} \quad (2)$$

“ c ” is soil cohesion, “ ϕ ” is the soil angle of friction (degrees), “ Z ” is the vertical coordinate direction (positive downward) and depth below the ground surface, “ t ” is the elapsed time since the start of storm, “ γ_w ” is unit weight of groundwater [kN/m^3], “ γ_s ” is soil unit weight [kN/m^3].

Study area: Serra do Mar—Copebrás Basin

The Serra do Mar has significant economic importance since it is crossed by the railway and highways that connect São Paulo and Rio de Janeiro, to their hinterland as well as to the port of Santos, the busiest in South America. At the foot of the Serra do Mar in São Paulo lies the

Cubatão region where Cubatão's Industrial Park houses one of Brazil's major petrochemical industries. Landslides and debris flow in the area have repeatedly caused major impacts to industries and infrastructure, because of landslides and debris flows due to the high, steep slopes covered by tropical residual soils from gneiss and colluvium, and intense rains that annually total 3000 mm but may reach 4500 mm.

In Brazil, the Serra do Mar escarpment extends for over 1500 km along the east coast and is one of the areas of the country most affected by mass movements, especially shallow landslides, which occur locally every year, causing environmental and social damage (Fig. 1a, b). Recent landslide disasters in Serra do Mar caused resulting in millions of dollars in economic losses and thousands of casualties and rendered thousands more homeless. Since the 1920s, there have been records of these processes, mainly debris flows and shallow landslides that caused casualties

especially during heavy rainfall (Costa Nunes 1986; Massad et al. 1997, 2000; Wolle and Carvalho 1989a, b).

A major landslide event occurred between January 23 and 24, 1985, when rain gauges recorded levels above 100 mm of rainfall per day. One gauge, for example, located beside the Moji River at 820 m a.s.l., recorded 379 mm in 48 h, accounting for between 40 and 60% of the month's total (Water Resource Management System of São Paulo State Department of Water and Power). This event caused around 1742 landslides (Fig. 2a), including large debris flow that reached major rivers and caused extensive flooding in low-lying areas occupied by residential and industrial structures. During this event, an industrial pipe containing ammonia broke, causing serious environmental and social damage to the region (Kanji et al. 1997, 2003; Lopes 2006; Massad et al. 2000).

In February 1994 (9 years later), a neighboring area closer to Cubatão was affected by landslides that reached

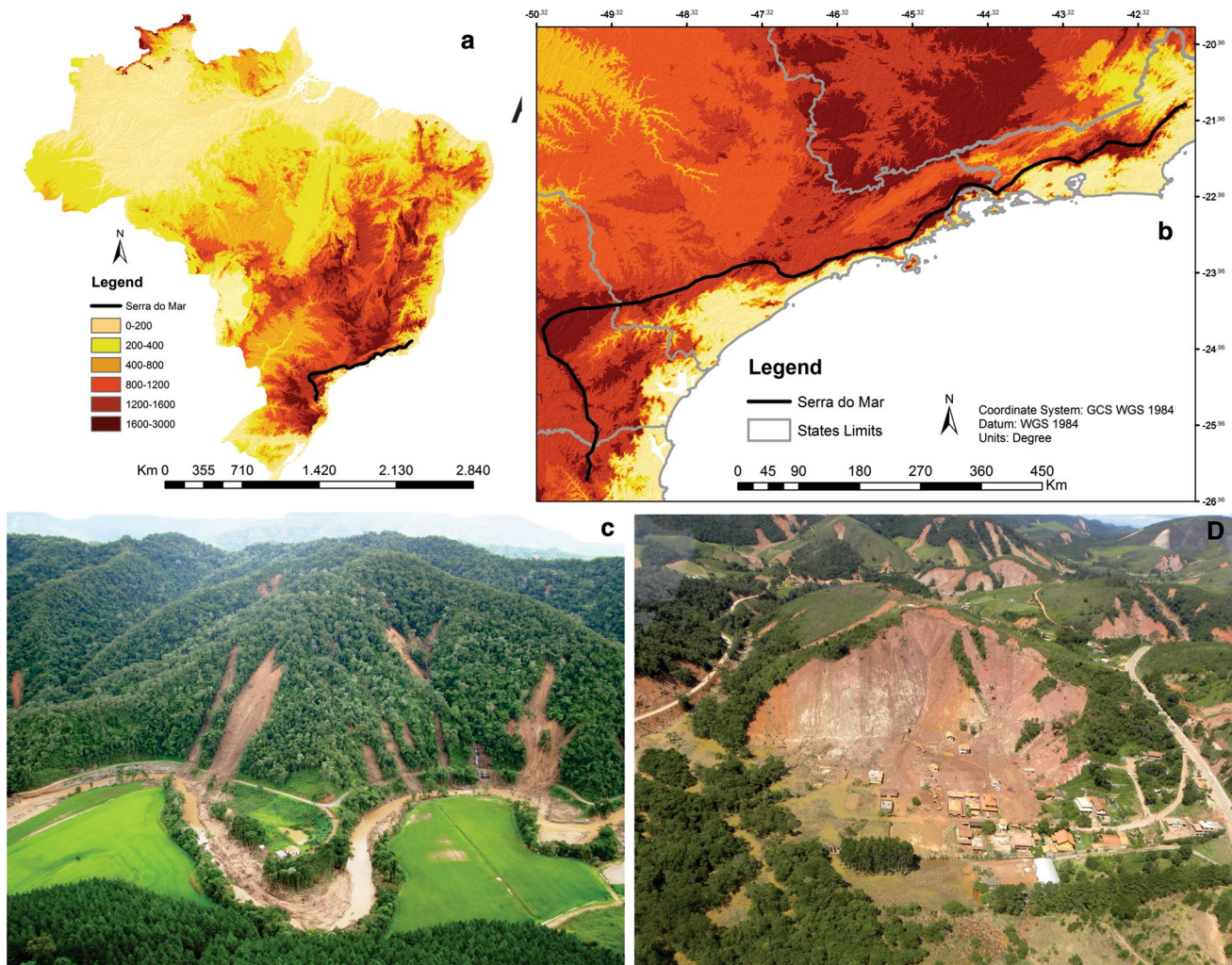


Fig. 1 Location of the Serra do Mar in Brazil (a, b). General mass-wasting that occurred in the Serra do Mar in 2008 (c) and 2011 (d) (photographs by Marcelo F. Gramani and Bianca Carvalho Vieira)

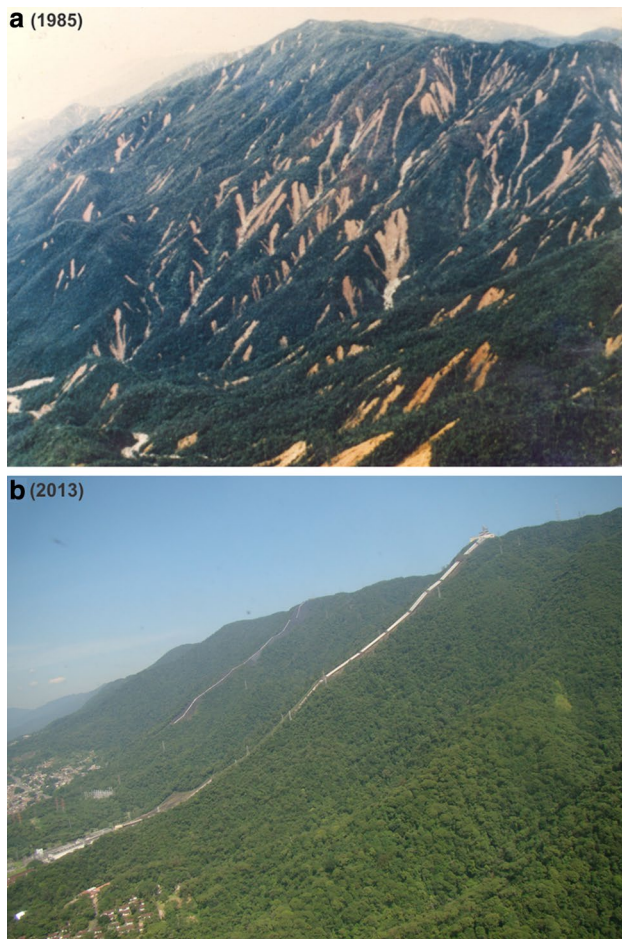


Fig. 2 **a** General view of the landslides that took place in Serra do Mar escarpment in 1985. **b** The same area in 2013, showing the residential sites and part of Cubatão's Industrial Park. Source: São Paulo State's Technological Research Institute

the main tributary streams, and coalesced into a debris flow with a volume estimated at about 300,000 m³ and velocity of around 10 m/s, that interrupted the Petrobrás oil refinery for about 3 weeks, leading to economic losses of about US\$40 million (Massad et al. 1997).

Heavy rains on November 22nd and 23rd, 2008, during, approximately 720 mm in 3 days, triggered large, deep landslides and mudflows (Fig. 1c), killing 135 people, displacing more than 80,000, and leaving 85 municipalities in a state of emergency and 14 in a state of public catastrophe (Vieira and Gramani 2015). After that, on January 11th and 12th, 2011, approximately eight municipalities in Serra do Mar (state of Rio de Janeiro) were affected by 3562 landslides (Fig. 1d). They were responsible for more than 1500 deaths and left nearly 20,000 homeless. The disaster followed an interval of heavy rains between October and December, culminating in approximately 300 mm over 48 h (Avelar et al. 2013).

We selected the 3.6 km² Copebrás Basin (Fig. 3) for analysis due to the presence of shallow landslides and because it is topographically representative of the region, as well as for its geographical position, near Brazilian Petrochemical Company (Copebrás), that was built in 1959 in Cubatão's Industrial Park. Geologically, the catchment's physical aspects are characterized by a predominance of migmatites (Embu Complex and Costeiro Complex), and the occurrence of biotite schist (Pilar Complex) at its base. Sixty percent of the hillslopes are between 400 m and 800 m in elevation, while 42% of the slope angles are between 30° and 40°. Hillslopes face mostly toward the SE, S, and SW (about 64%) and display predominantly convex (40%) and straight profiles (40%) with a smaller share of them concave (20%) (Vieira et al. 2010).

According to field investigations (Wolle and Carvalho 1989a, b) carried out in two areas next to Copebrás Basin with slopes between 40° and 43°, there are two types of regolith above the intensely fractured bedrock: *colluvial soil* (about 1 m depth) formed by pedogenesis over transported material, with a sandy-clayey texture matrix and partially weathered bedrock; and *saprolite* (about 3 and 4 m depth), more sandy than the overlying horizon, with evidence of structures inherited from bedrock (Table 1, Fig. 4).

Methodology

Simulation of susceptibility scenarios

The topographical input to both models was generated from a 4-meter-grid digital elevation model (DEM) obtained from a topographical map (1:10,000 scale) and interpolated using the *Topo to Raster* module of ArcGIS 9.1. The *Topo to Raster* module is an interpolation method specifically designed for the creation of hydrologically correct digital elevation models (DEMs), imposing constraints that ensure a connected drainage structure and correct representation of ridges and streams from input contour data.

In the TRIGRS model, the DEM was used to implement the runoff-routing scheme that uses the weighting factors for runoff distribution by TopoIndex (*Topographical Index*). In this paper, we used the “D8 flow direction” that considers the maximum runoff-routing, where the “water flows down the steepest slope, computes the direction of steepest slope and attempts to direct flow in that direction by partitioning the flow between the two cells nearest to the steepest slope direction (Baum et al. 2002)”. Alternative options for runoff-routing include: (1) divert excess water only to the adjacent cell on the steepest downslope path; (2) distributes the excess water evenly among all adjacent downslope cells; this pattern has the greatest dispersion of all the choices and

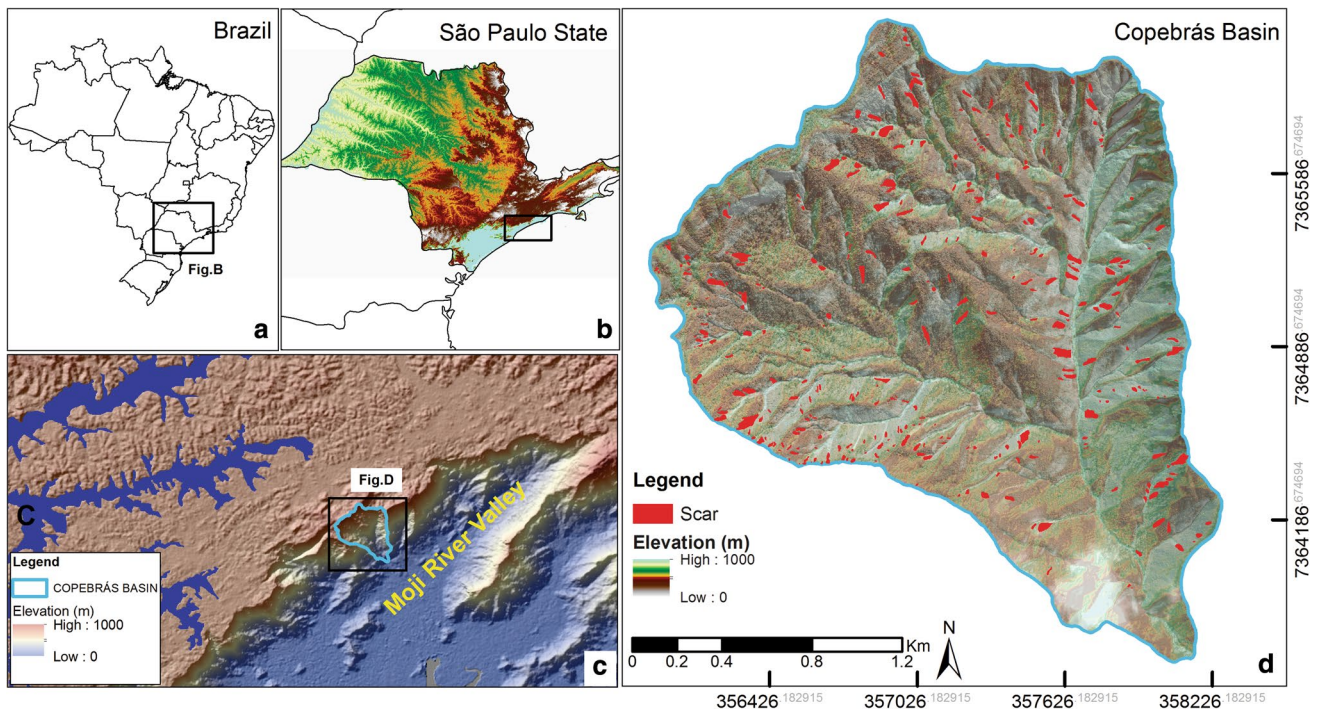


Fig. 3 Location of the Copebrás Basin in the Serra do Mar, São Paulo State, Brazil (a, b). The Copebrás basin with landslide scars triggered during the rainfall between January 23 and 24, 1985 (c, d)

Table 1 Values of field investigations: “ γ_s ” is the soil unit weight [kN/m³]; “c” is the soil effective cohesion [Pa]; and “ ϕ ” is the soil angle of friction [°]. Highlighting shows the values used in the scenarios, as representative for the Serra do Mar region

Site/soil thickness (m)	A1			A2		
Parameters	γ_s [kN/m ³]	c [Pa]	ϕ [°]	γ_s [kN/m ³]	c [Pa]	ϕ [°]
Colluvial soil (1 m)	14.3–17.1	1000–6000	34	16.5–18.2	1000–9500	36–40
Saprolite (1–2 m)	18–19.5	4000–12,000	39–45	18.5–20.1	3500–11,000	39–45

Modified from (Wolle and Carvalho 1989)

(3) flow is distributed among all downslope cells in proportion to the slope.

Based on geotechnical and hydrological parameters obtained by Wolle and Carvalho 1989a, b (Fig. 4) two groups of scenarios were simulated considering the minimum (Scenario A) and maximum (Scenario B) values of *Colluvial soil* (Soil cohesion and Total unit weight of soil) (Table 2). In those scenarios, soil thickness (z) of 1, 2, and 3 m were used to generate three runs for each scenario: A1, A2, and A3 and B1, B2, and B3, respectively. In the two models, we used the lowest value of internal friction angle (34°) based on Table 2. This value corresponds to the mean value reported by other studies carried out in nearby areas with similar geological and geomorphological conditions, which obtained a range between 20° and 40° (De Campos 1992; de Ploey and Cruz 1979; Guimarães et al. 2003). No soil depth maps are available for the Serra do Mar.

In the TRIGRS model the “initial height of the water table (d)” was the “soil maximum thickness (Z_{max})” and constant values were used in all simulated scenarios for the Initial infiltration rate (I_{LT}), hydraulic diffusivity (D_0) and vertical saturated hydraulic conductivity (K_s). For the first two parameters, we used the default values of TRIGRS, except the K_s that was based on data collected using the Guelph Permeameter in three scars in an experimental basin located in the Serra do Mar. In this investigation, 80% of K_{sat} values concentrated between 10^{-6} and 10^{-5} m/s. For the rainfall parameters (number of events, rain intensity, and duration of each event), we used three events each of which lasted for 6 h, between 23 and 24 January 1985 (Table 3).

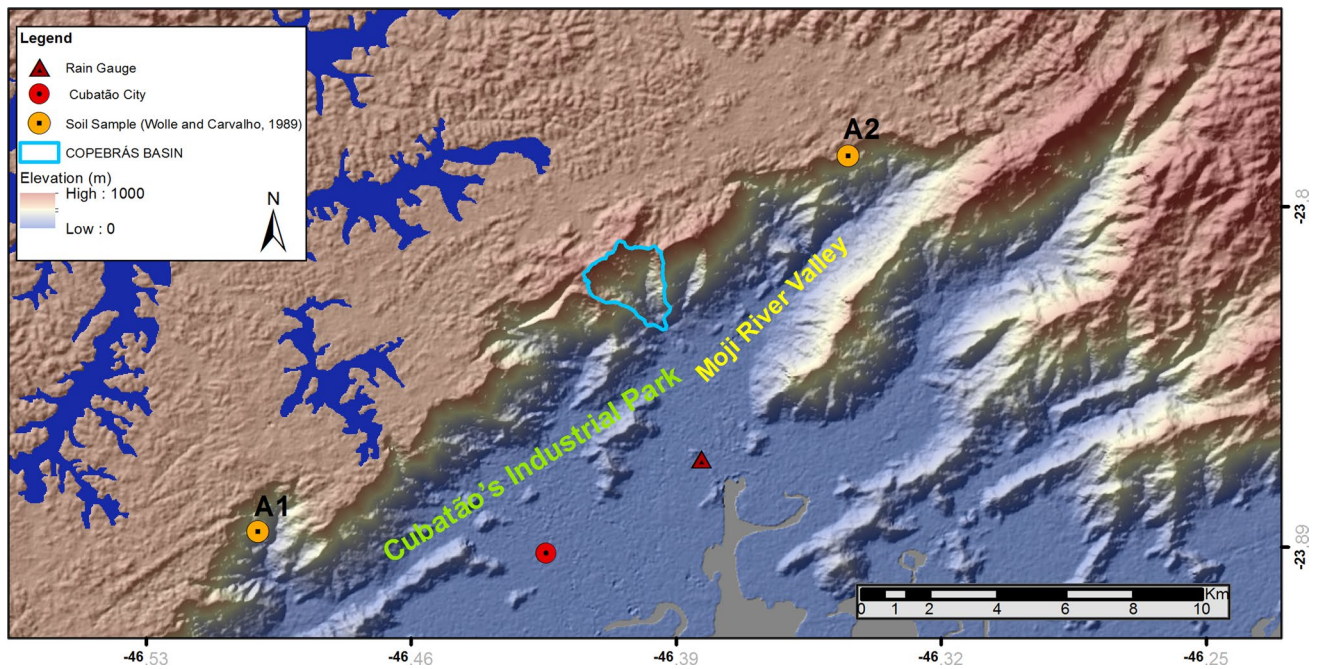


Fig. 4 Location of collected samples (A1 and A2) by Wolle and Carvalho (1989) and Rain Gauge used for the evaluation of rainfall data used in the model TRIGRS

Table 2 Mechanical and hydrological parameters used in Scenarios A and B

Scenarios	Scenario A			Scenario B		
	A1	A2	A3	B1	B2	B3
Parameters [unit]						
Soil cohesion ^a (c) [Pa]	1000	1000	1000	6000	6000	6000
Total unit weight of soil ^a (γ_s) [kN/m ³]	17.1	17.1	17.1	14.3	14.3	14.3
Soil maximum thickness ^a (Z_{max}) [m]	1	2	3	1	2	3
Internal angle of friction ^a (Φ) [°]	34	34	34	34	34	34
Initial height water table. (d) [m]	1	2	3	1	2	3
Initial infiltration rate ILT [m/s]	1.0×10^{-9}	1.0×10^{-9}	1.0×10^{-9}	1.0×10^{-9}	1.0×10^{-9}	1.0×10^{-9}
Hydraulic diffusivity D_0 [m ² /s]	5.5×10^{-4}	5.5×10^{-4}	5.5×10^{-4}	5.5×10^{-4}	5.5×10^{-4}	5.5×10^{-4}
Vertical saturated hydraulic conductivity (K_v) [m/s]	1.0×10^{-6}	1.0×10^{-6}	1.0×10^{-6}	1.0×10^{-6}	1.0×10^{-6}	1.0×10^{-6}

^aParameters used in model SHALSTAB

Table 3 Rainfall parameters of three events which lasted for 6 h (23 and 24 January, 1985) *Source data:* São Paulo’s integrated water resource management system of São Paulo state department of water and power

Accumulated duration at the end of each event in s (h)	Average rain intensity for each event, I_{nz} (m/s)
0 s (0 h)	5.4×10^{-7}
21,600 s (6 h)	1.7×10^{-6}
43,200 s (12 h)	6.0×10^{-6}

Landslide maps and parameter evaluation

Landslide scars were mapped on 1:25,000 aerial photographs taken 3 months after the 1985 event. The scars were identified based on visual analysis of the features, using the following criteria: geometry, the absence of vegetation, contour lines and texture analysis and hillslope position (Fig. 5). As found in other studies in the Serra do Mar, shallow landslide failures occur in the upper portions of

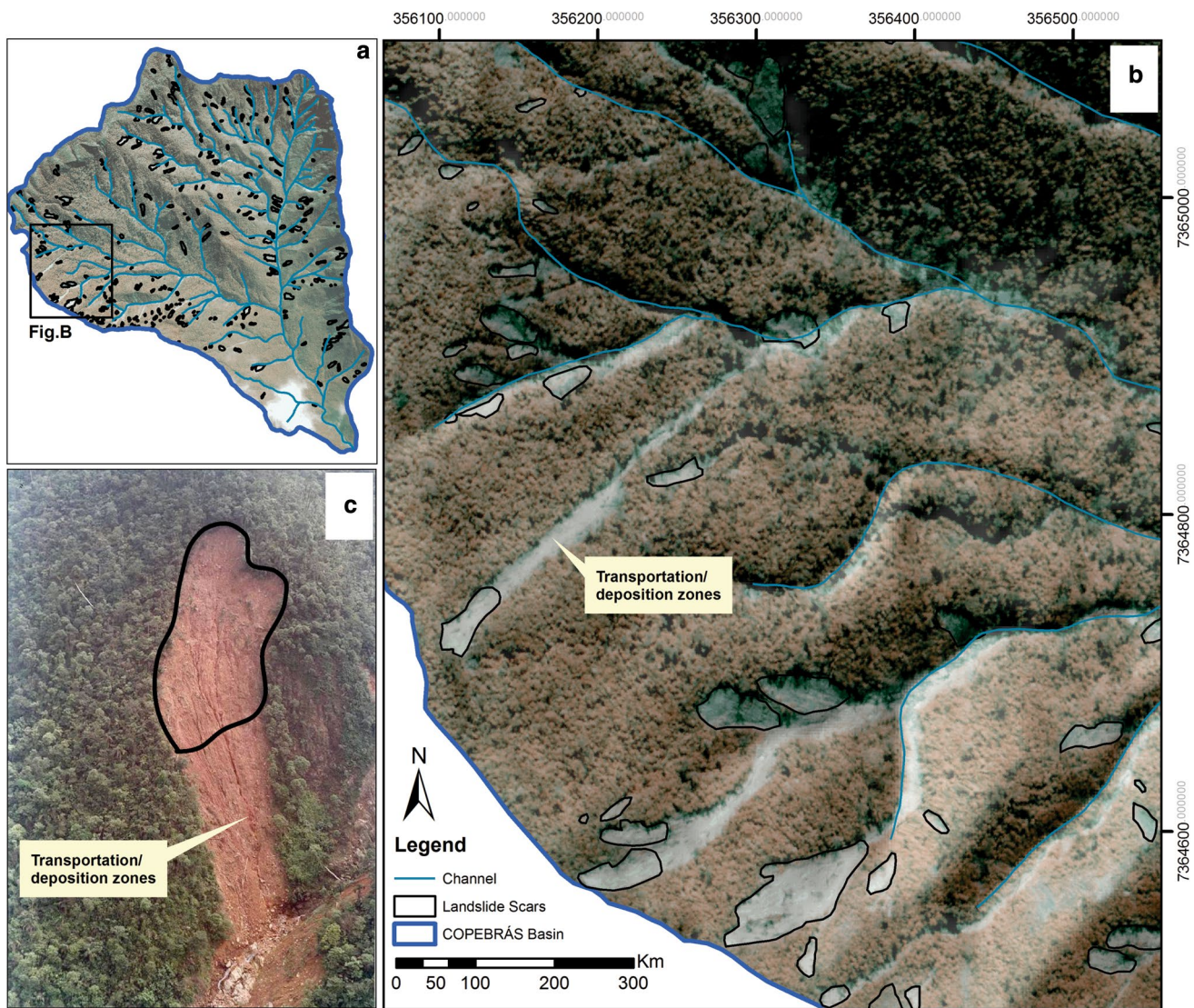


Fig. 5 **a** Scar landslides map; **b** part of landslide scars map considering only the upper part of the scars; and **c** example of the part of the scar mapped and the zones of transportation and deposition

the hillslopes, with the middle and bottom portions of scar being areas of transportation and deposition.

We mapped 356 scars from the 1985 event that altogether represent about 3.7% of the total area of the basin. Most of the scars (213) occupied an area of less than 300 m². The largest mapped scar had an area of 2704 m² while the smallest involved only 11 m² (Fig. 6).

We used this landslide scar map to evaluate the performance of the susceptibility maps and using two indexes (Gao 1993): (1) Scar Concentration (SC), the ratio of the number of cells in each susceptibility class affected by shallow landslides to the total number of cells in the basin; and (2) landslide potential (LP), the ratio of the number of cells in each susceptibility class affected by the shallow landslides to the total number of cells in the same susceptibility class. For

both models, we also produced the frequency (*F*) histogram of the number of cells of each susceptibility class: the ratio between the number of cells in each susceptibility class and the total number of cells in the basin (Table 4).

Also, for both models, we determined two metrics of spatial correspondence between observed landslide scars and predicted zones of landsliding: (1) areas of predicted landslide susceptibility where no landslides occur; and (2) areas where landslide scars occur in locations predicted to be stable. Due to the differences in the susceptibility outputs in the TRIGRS model the first two classes (between 0.4 and 0.8 and between 0.8 and 1.0) were considered to be unstable ($F_s \leq 1$) and in the SHALSTAB, only the “Unconditionally Unstable” were considered to be unstable and only “Unconditionally Stable” like stable areas. Thus, even though the

Fig. 6 Size distribution of landslide scars (m^2). Most of the scars were under 200 m^2 , not including mapped areas of transportation and deposition; over 100 scars have an area greater than 400 m^2

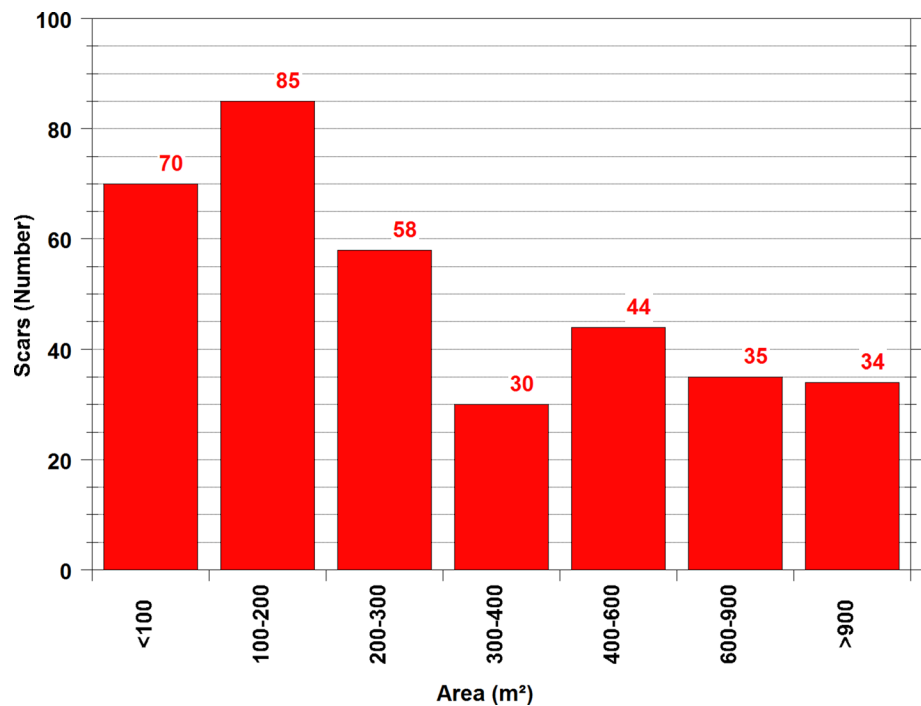


Table 4 Example illustrating the calculation of the scar concentration (SC) and the landslide potential (LP) indices

Classes	Pixel	Pixel with Scars	F (%)	SC (%) = $C3/33,168 \times 100$	LP (%) = $C3/C2 \times 100$
Unc. unstable	288,757	17,253	32.4	$17,253/33,168 = 52.0$	$17,253/288,757 = 6.0$
< -3.1	113,471	3939	12.7	$3939/33,168 = 11.9$	$3939/113,471 = 3.5$
-3.1 to -2.8	83,562	2689	9.4	$2689/33,168 = 8.1$	$2689/83,562 = 3.2$
-2.8 to -2.5	112,125	3455	12.6	$3455/33,168 = 10.4$	$3455/112,125 = 3.1$
-2.5 to -2.2	114,137	2804	12.8	$2804/33,168 = 8.5$	$2804/114,137 = 2.5$
> -2.2	123,172	2555	13.8	$2555/33,168 = 7.7$	$2555/123,172 = 2.1$
Unc. stable	55,857	473,00	6.3	$473,00/33,168 = 1.4$	$473,00/55,857 = 0.8$
Total	891,081	33,168	100	100	3.72%

intermediate classes SHALSTAB may indicate potentially unstable areas in the landscape, here they were not considered for this validation.

Results

Susceptibility maps derived from the TRIGRS model

In scenarios A1, A2 and A3 (Fig. 7), few variations were identified in the spatial distribution of susceptibility classes. That is, as soil depth increased from 1 m (A1) to 2 m (A2), the unstable areas experienced a 10% increase. Between 2 m (A2) and 3 m (A3), this increase was only 3%.

The most unstable class (0.4 and 0.8) occupied 9 to 18% of the area, whereas the next class (0.8 and 1.0) occupied approximately 25%. The first two classes (all unstable

areas, with $F_s \leq 1$) occupy approximately the following percentages of the area: 33% (A1), 40% (A2) and 43% (A3). The stable areas occupied 67% (A1), 60% (A2) and 57% (A3).

Different geotechnical and hydrological parameters in scenarios B1, B2, and B3 resulted in important differences, increasing the percentage of stable areas in the three scenarios (Fig. 8a). In scenario B1, 100% of the basin was classified as stable, in B2 97% and in B3 87%. Thus, in group B, the three scenarios had higher SC class stability, with only a few scars (<5%) in scenario B3.

Figure 8b shows that the lowest F_s (between 0.4 and 0.8) is also associated with lower values of SC: 13% (A1), 24% (A2) and 38% (A3). However, the next class (0.8 and 1.0) had higher but consistent SC values: 40% (A1), 40% (A2) and 39% (A3). The classes with $F_s < 1$ had the following CC values: 53% (A1), 63% (A2) and 66% (A3).

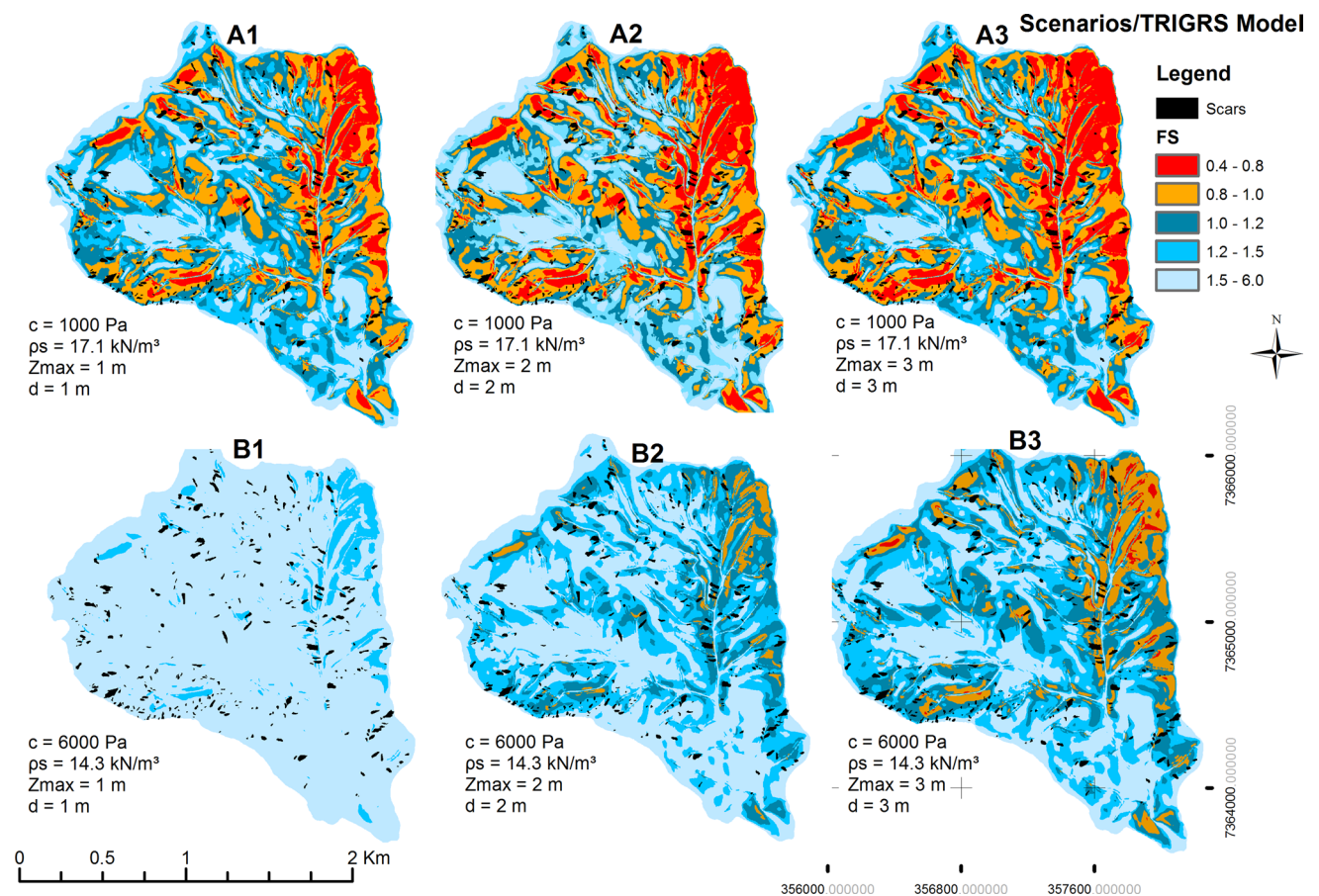


Fig. 7 Susceptibility maps produced by the TRIGRS model under different conditions of cohesion, the angle of friction and soil thickness (Scenarios A and B). The scenarios from group A (above) differ from those of group B (below) because of an increase in stable classes in group B

Susceptibility maps derived from the SHALSTAB model

Similar to the results of the TRIGRS model, there was a strong similarity in the spatial distribution of susceptibility classes for group A (Fig. 9). The most significant change (an increase of approximately 10%) occurred between scenarios A1 and A2 (Fig. 9a).

In those scenarios, analyzing only the Unconditionally Unstable class, the frequency (F) had exactly the same percentage values as the unstable classes ($F_s < 1$) in the TRIGRS model: 33% (A1), 40% (A2) and 43% (A3). We note that the SHALSTAB model also showed that modifying the geotechnical and hydrological parameters led to changes in the unstable and stable classes. In the simulation, setting soil thickness equal to 1 m (B1) resulted in the whole basin being classified as Unconditionally Stable.

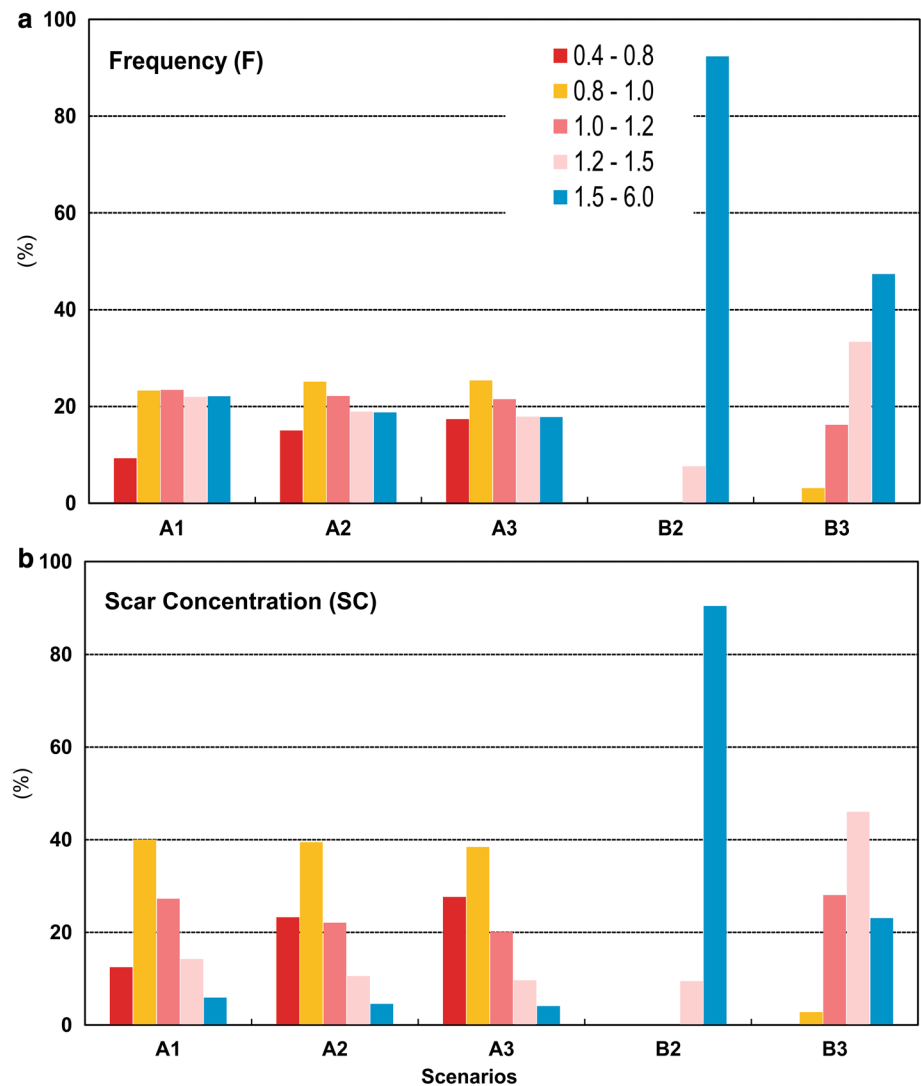
The scar concentration (SC) in the three scenarios shows that there is a similar distribution of shallow landslides in each of the susceptibility classes (Fig. 10b). However, we highlight the scar percentage in the Unconditionally

Unstable class in the scenarios (between 53 and 66%). Considering scenario A3, for example, where cumulative percentages reached almost 90% CC, 76% of the scars were concentrated on log class $(q/T) - 3.1$, 82% < of the scars were concentrated in $\log (q/T) - 2.8$, and 89% < of the scars were concentrated in $\log (q/T) < -2.5$. In scenarios B2 and B3, only 2.3 and 17% of the total number of scars, respectively, occurred in unstable areas (Fig. 10b).

LP index comparison between SHALSTAB and TRIGRS

The relationship between the susceptibility maps and the scar map of 1985 can be evaluated using the *landslide potential index* (LP). In the TRIGRS model (Fig. 11a), the first two classes ($F_s < 1$) had high LP values. The class from 0.4 to 0.8 had the following LP values: 5.0% (A1), 5.7% (A2), and 5.9% (A3), and the class between 0.8 and 1.0 had the following LP values: 6.4% (A1), 5.8% (A2), and 5.6% (A3). In contrast, the classes with $F_s > 1$ had lower values, below 1%.

Fig. 8 **a** The Frequency (F) is similar in the A scenarios, but there is a significant reduction in unstable classes in the B scenarios. **b** The highest scar concentration (SC) occurred between 0.8 and 1.0, reaching approximately 40% in all scenarios



In the B scenarios, the most unstable classes (between 0.4 and 0.8 and between 0.8 and 1.0) exhibited LP values below 3%. One exception was the class between 0.8 and 1.0 in scenario B3, which reached an LP value of approximately 6%, equal to that of scenario A2. However, in general, stable classes had the highest LP values.

In the SHALSTAB model (Fig. 11b), the highest LP values were recorded for the Unconditionally Unstable class. In all scenarios except B1 and B2, there was a tendency toward a decrease in the number of stable classes. At first, the entire area was designated as stable, and scenario B2 showed the opposite trend in LP values, which increased with the number of stable classes.

Unstable areas without scars and stable areas with scars

Due to differences between the susceptibility classes of the models, unstable areas in the TRIGRS model were

regarded to be the sum of the first two classes (0.4–0.8 and 0.8–1.0) and stable areas were regarded to be the sum of the last three (1.0–7.0). The SHALSTAB model classes *Unconditionally Unstable* and *Unconditionally Stable* were used to calculate unstable and stable areas, respectively.

According to Fig. 12, there were no substantial differences between the two groups of scenarios in both models. The largest differences occurred between the scenario A and B groups because a larger area was occupied by unstable classes in scenarios A1, A2 and A3 relative to scenarios B1, B2 and B3.

Both models resulted in scenarios with 30–40% of unstable areas with the scar landslides from 1985. However, the percentage of stable areas with scars was very low in all scenarios for both models. These percentages demonstrate that the models perform well in predicting areas that are susceptible to shallow landslides. The large percent of areas in the B scenarios that were predicted to be stable scars was

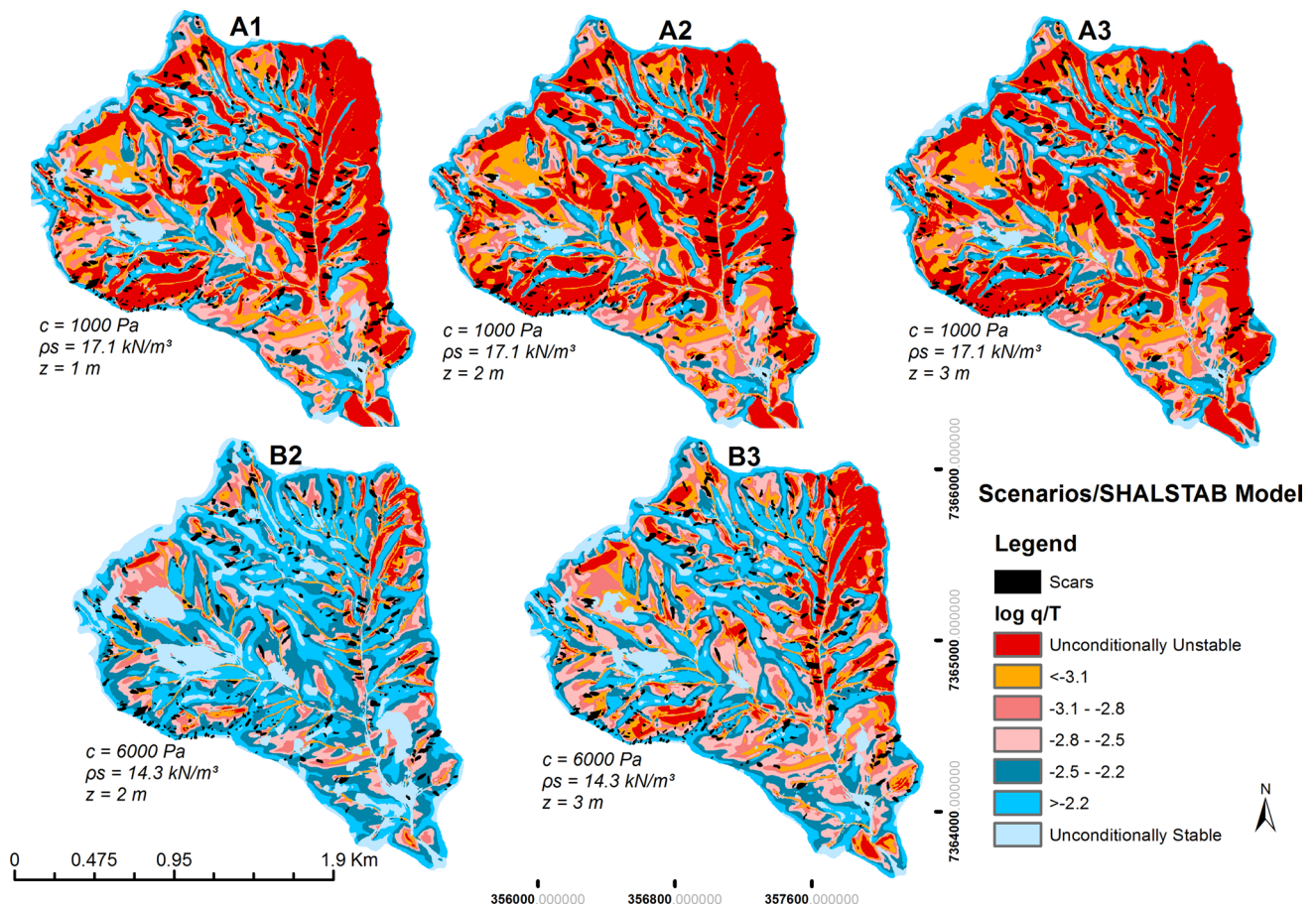


Fig. 9 Susceptibility maps generated by the SHALSTAB model under different conditions of cohesion, friction angle, and soil thickness. There is little difference in the distribution of classes in the various scenarios and a significant increase in the stable class in group B

expected based on the results of the frequency and scar concentration indices.

Discussion

More significant differences were found between scenarios A and B than between the susceptibility maps generated by the two models.

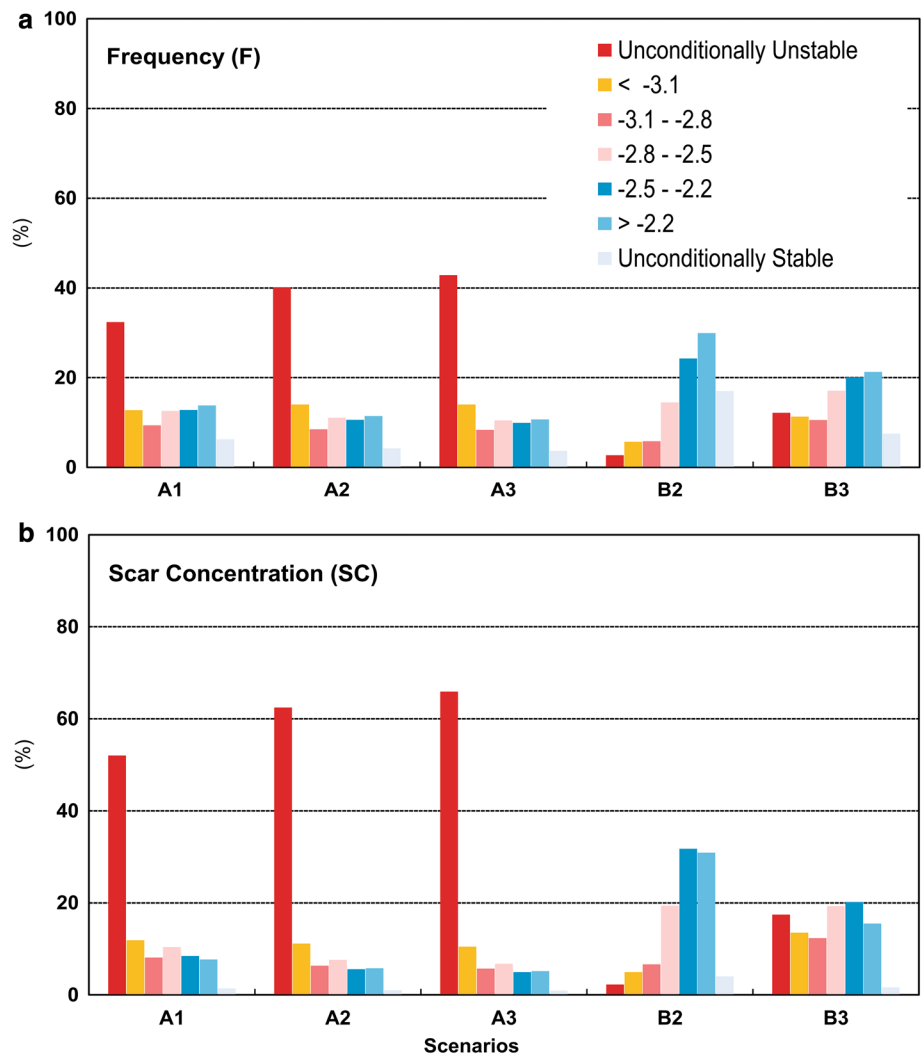
The spatial distribution of unstable and stable areas was controlled by topographical variables, particularly the slope angle and slope form. Stable areas appeared as smooth sections on top of the main convex slopes with interfluvial angles over 30°, whereas the unstable areas were higher (over 400 m) and steeper (>40°). In the lower portion of the basin, near the mouth of the main river, an increase in stable areas was observed due to the presence of gentle interfluvial (<30°) and only a small area at the bottom of the basin within the main drainage bottleneck was classified as unstable due to higher slope angles (>40°).

The cumulative percentage of SC in each susceptibility class reached values similar to those found by Montgomery and Dietrich (1994), approximately 90% in $\log(q/T) < 2.5$. Even though the areas are quite different, the Serra do Mar also exhibits shallow soils over bedrock with flow into the highly weathered, fractured regolith.

Somewhat smaller cumulative percentages were obtained by Dietrich and Montgomery (1998), who identified only 54% of the landslides in $\log(q/T) < -3.1$ and 68% in $\log(q/T) < -2.8$. Considering cumulative percentages and the limits of $\log(q/T)$, Dietrich et al. (1998) attributed variation between SCs to the quality and resolution of the DEM grid. According to those authors, to capture more than 60% of the scars in a grid of $\log(q/T) < -2.5$ for a 10-m grid, a limit of $\log(q/T) < -2.8$ is necessary. With a high-resolution grid, the limit can reach $\log(q/T) < -3.1$. Based on these results, using a 4-m resolution in the present study makes it possible to capture over 60% of the scars in the limit of $\log(q/T) < -3.1$.

Dietrich et al. (1998) determined this relationship from studies in different basins with 844 landslides triggered

Fig. 10 **a** The frequency (F) is similar between scenarios, but there is a significant reduction in unstable classes in the B scenarios. **b** The highest scar concentration (SC) occurred between 0.8 and 1.0, reaching approximately 40% in all scenarios



between 1978 and 1996. Using a DEM with a resolution of 10 m^2 , they observed that on average, approximately 46% of these cases occurred in the two lower instability classes, Unconditionally Unstable and $\log(q/T) < -3.1$. Using a DEM of 2 m^2 , approximately 94% of the scars coincided with the Unconditionally Unstable class.

In Brazil, similar results were found by Guimarães et al. (2003), in applying SHALSTAB in two basins with similar geomorphological and geological conditions. They simulated scenarios of susceptibility using cohesion values between zero and 20 kPa. In the best-performing scenarios, with zero soil cohesion, 79% of the scars coincided with the $\log(q/T) - 2.8$ class and 91% in $\log(q/T) < -2.5$ class. Using cohesion values between 10 and 20 kPa, only 37% of the scars coincided with the $\log(q/T) < -2.8$ class. These authors argued that the best performance occurring with no cohesion showed the importance of topographical control on triggering shallow landslides.

Previous studies that compared the two models also did not identify important differences between the susceptibility

maps (Baum et al. 2005; Savage et al. 2004). These studies showed that the similar spatial distribution of unstable areas suggested by models is associated with strong topographical control. This result held even though soil thickness was considered to be constant over the entire area in the SHALSTAB model, whereas the TRIGRS model used distinct soil thickness values derived from geological and geotechnical maps.

In other studies that compared the SHALSTAB and TRIGRS models, some authors concluded that the SHALSTAB model overestimated unstable areas (Crosta et al. 2003; Fratini et al. 2004), while SHALSTAB showed that 46% of the area was unstable, the TRIGRS model predicted only 17.5%.

It is important to note, however, that the SHALSTAB model was designed to consider potentially unstable areas regardless of rainfall volume and intensity. Areas of potentially unstable terrain are identified in terms of increasing amounts of rainfall being necessary to trigger instability in different potential instability classes. In contrast, the TRIGRS model was intended to simulate stable areas under specific rainfall conditions, which are provided during the

Fig. 11 LP Index of the TRI-GRS (a) and SHALSTAB (b) models

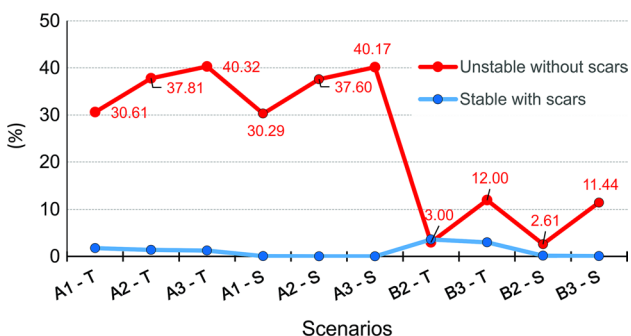
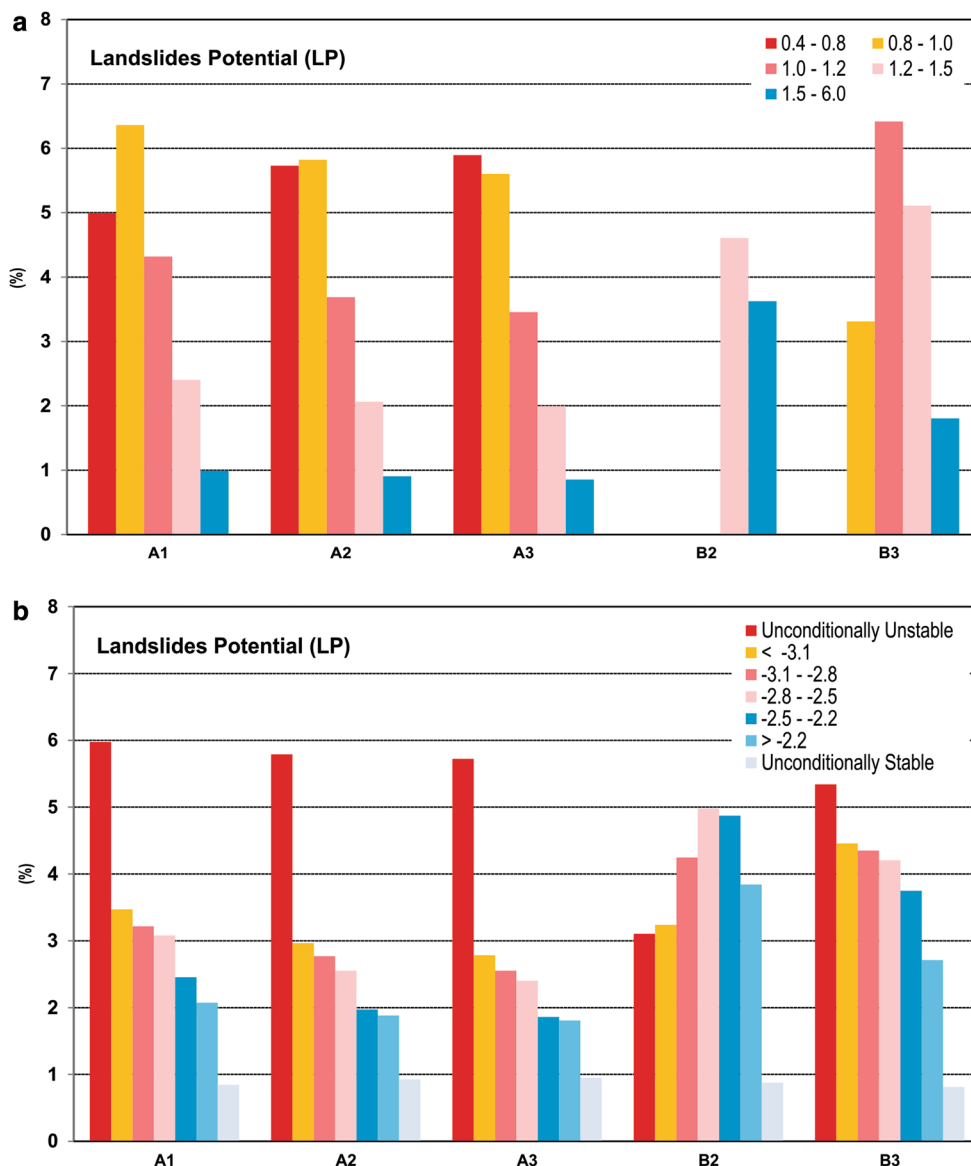


Fig. 12 The red line indicates the percentage of unstable areas without scars, and the blue line indicates stable areas with scars from the January 1985 event (S indicates SHALSTAB and T indicate TRI-GRS)

processing of the susceptibility scenarios. We suggest that this potential overestimation from the SHALSTAB model must be weighted because the model identifies only *potentially* unstable areas. The areas that do not have scars and are designated to be potentially unstable can be triggered under higher-intensity rainfall conditions other than those recorded in January 1985.

As shown in Fig. 11, unstable areas without scars in the SHALSTAB model cannot be evaluated because the model indicates only potentially unstable areas. In contrast, the TRIGRS model calculates the spatial variation of the F_s for a specific rainfall type and amount such as that we used in this paper. Therefore, the models' efficiency should be compared in addition to the differences between them that may indicate different instabilities; for example, considering time or a specific rainfall that triggers shallow landslides.

Conclusions

- Both SHALSTAB and TRIGRS models were shown to be effective in predicting shallow landslides through comparison of areas predicted to be unstable and locations of mapped landslides and through the use of Landslide Potential index.
- Differences in model performance between scenarios A and B, due to differences in effective cohesion and soil thickness values, can help evaluate appropriate values of geotechnical data (e.g., soil property) to incorporate into regional susceptibility maps.
- Due to the satisfactory results in this study, even through the use of secondary data, either model appears useful for governmental agencies interested in low-cost methods for identifying potentially unstable areas, mainly where obtaining data in the field are costly and difficult.

Acknowledgements The authors thank the journal editor and the reviewers, the São Paulo Research Foundation (FAPESP 2014/10109-2), the Coordination for the Improvement of Higher Education Personnel (CAPES BEX 5188/14-8) and FACEPE (BFP-0072-1.07/16) for partial financial support for this research. We are grateful to those who spent the time Dr^a. Lupamudra Dasgupta e a Harvey Greenberg (GisLAB, University of Washington).

References

- Avelar AS, Coelho Netto AL, Lacerda WA, Becker LB, Mendonça MB (2013) Mechanisms of the recent catastrophic landslides in the mountainous range of Rio de Janeiro, Brazil. In: Margottini C, Canuti P, Sassa K (eds) *Landslide Science and Practice*, vol 4. Springer, Berlin
- Baum RL, Savage WZ, Godt JW (2002) TRIGRS: a Fortran program for transient rainfall infiltration and grid-based regional slope-stability analysis. USGS, Colorado
- Baum RL et al (2005) Regional landslide-hazard assessment for Seattle, Washington, USA. *Landslides* 2:266–279. <https://doi.org/10.1007/s10346-005-0023-y>
- Costa Nunes AJ (1986) Formação, Classificação e Comportamento de Depósitos de Encostas no Sudeste Brasileiro - Estabilização de Taludes nas Encostas da Serra do Mar
- Crosta GB, Dal Negro P, Frattini P (2003) Soil slips and debris flows on terraced slopes. *Nat Hazards Earth Syst Sci* 3:31–42
- De Campos TMP, Vargas Jr., E.A., Eisenstein, Z. Considerações Sobre Processos de Instabilização de Encostas em Solos não Saturados na Cidade do Rio de Janeiro. In: 1^a Conferência Brasileira Sobre Estabilidade de Encostas - 1^a COBRAE, Rio de Janeiro, 1992. pp 741–757
- de Ploey J, Cruz O (1979) Landslides in the Serra do Mar. Brazil CAT-ENA 6:111–122. [https://doi.org/10.1016/0341-8162\(79\)90001-8](https://doi.org/10.1016/0341-8162(79)90001-8)
- Dhakal AS, Sidle RC (2003) Long-term modelling of landslides for different forest management practices. *Earth Surf Proc Land* 28:853–868. <https://doi.org/10.1002/esp.499>
- Dietrich WE, Montgomery DR (1998) SHALSTAB: a digital terrain model for mapping shallow landslide potential. National Council of the Paper Industry for Air and Stream Improvement
- Dietrich WE, Wilson CJ, Montgomery DR, McKean J (1993) Analysis of erosion thresholds channel networks, and landscape morphology using a digital terrain model. *J Geol* 101:259–278. <https://doi.org/10.1086/648220>
- Dietrich WE, Reiss R, Hsu M-L, Montgomery DR (1995) A process-based model for colluvial soil depth and shallow landsliding using digital elevation data. *Hydrol Process* 9:383–400. <https://doi.org/10.1002/hyp.3360090311>
- Dietrich WE, Asua RRd, Orr JCB, Trso M (1998) A validation study of the shallow slope stability model, SHALSTAB, in forested lands of Northern California. Stillwater Ecosystem, Watershed & Riverine Sciences, Berkeley, CA
- Frattini P, Crosta GB, Fusi N, Dal Negro P (2004) Shallow landslides in pyroclastic soils: a distributed modelling approach for hazard assessment. *Eng Geol* 73:277–295. <https://doi.org/10.1016/j.enggeo.2004.01.009>
- Gao J (1993) Identification of topographic settings conducive to landsliding from dem in Nelson County, Virginia, USA. *Earth Surf Process Landf* 18:579–591
- Guimarães RF, Montgomery DR, Greenberg HM, Fernandes NF, Trancoso Gomes RA, de Carvalho AO (2003) Parameterization of soil properties for a model of topographic controls on shallow landsliding: application to Rio de Janeiro. *Eng Geol* 69:99–108. [https://doi.org/10.1016/s0013-7952\(02\)00263-6](https://doi.org/10.1016/s0013-7952(02)00263-6)
- Guzzetti F, Carrara A, Cardinali M, Reichenbach P (1999) Landslide hazard evaluation: a review of current techniques and their application in a multi-scale study. *Central Italy Geomorphol* 31:181–216. [https://doi.org/10.1016/s0169-555x\(99\)00078-1](https://doi.org/10.1016/s0169-555x(99)00078-1)
- Iverson RM (2000) Landslide triggering by rain infiltration. *Water Resour Res* 36:1897–1910. <https://doi.org/10.1029/2000wr900090>
- Kanji MA, Cruz PT, Massad F, Araújo Filho HA (1997) Basic and common characteristics of debris flows. In: 2a Conferência Brasileira sobre Estabilidade de Encostas 2nd Pan-American Symposium on Landslides, Rio de Janeiro. pp 223–231
- Kanji MA, Massad F, Cruz PT (2003) Debris flows in areas of residual soils: occurrence and characteristics. In: *Associazione Geotecnica Italiana international workshop on occurrence and mechanism of flows in natural slopes and earthfills*, Naples. pp 1–9
- Lopes ESS (2006) Modelagem Espacial Dinâmica em Sistema de Informação Geográfica: Uma Aplicação ao Estudo de Movimentos de Massa em Uma Região da Serra do Mar Paulista. Universidade Estadual Paulista
- Massad F, Cruz PT, Kanji MA (1997) Comparison between estimated and measured debris flow discharges and volume of sediments. In: 2a Conferência Brasileira sobre Estabilidade de Encostas/2nd Pan-American Symposium on Landslides, Rio de Janeiro. pp 213–222
- Massad F, Cruz PT, Kanji MAE, Araujo Filho HA (2000) Characteristics and volume of sediment transported in debris flows in Serra do Mar, Cubatão, Brasil. In: *International workshop on debris flow disaster of December 1999 in Venezuela, Caracas, Venezuela*
- Montgomery DR, Dietrich WE (1994) A physically based model for the topographic control on shallow landsliding. *Water Resour Res* 30:1153–1171. <https://doi.org/10.1029/93wr02979>
- Montgomery DR, Sullivan K, Greenberg HM (1998) Regional test of a model for shallow landsliding. *Hydrol Process* 12:943–955. [https://doi.org/10.1002/\(sici\)1099-1085\(199805\)12:6%3c943:aid-hyp664%3e3.0.co;2-z](https://doi.org/10.1002/(sici)1099-1085(199805)12:6%3c943:aid-hyp664%3e3.0.co;2-z)
- Montrasio L, Valentino R (2008) A model for triggering mechanisms of shallow landslides. *Nat Hazards Earth Syst Sci* 8:1149–1159. <https://doi.org/10.5194/nhess-8-1149-2008>
- Morrissey MM, Wiczorek GF, Morgan BA (2001) A comparative analysis of hazard models for predicting debris flows in Madison County, VA, Version 1.0 edn.
- Pack RT, Tarboton DG, Goodwin CN (1998) *Terrain Stability Mapping with SINMAP, technical description and users guide for version 1.00*. Terratech Consulting Ltd., Salmon Arm, B.C., Canada

- Savage WZ, Godt JW, Baum RL (2004) Modeling Time-Dependent Aerial Slope Stability. In: Proceedings of 9th International Symposium on Landslides, vol 1. Landslides-Evaluation and Stabilization, Rio de Janeiro, RJ, Brazil, pp 23–36
- Sidele RC, Wu W (1999) Simulating effects of timber harvesting on the temporal and spatial distribution of shallow landslides. *Zeitschrift für Geomorphologie* 43:185–201
- van Westen CJ (2004) Geo-information tools for landslide risk assessment: an overview of recent development. In: Group TF (ed) Landslides: evaluation and stabilization. Taylor & Francis Group, Rio de Janeiro, pp 39–53
- Vieira BC, Gramani MF (2015) Serra do Mar: the most “tormented” relief in Brazil. *Landsc Landf Brazil*. https://doi.org/10.1007/978-94-017-8023-0_26
- Vieira BC, Fernandes NF, Filho OA (2010) Shallow landslide prediction in the Serra do Mar, São Paulo, Brazil. *Nat Hazards Earth Syst Sci* 10:1829–1837. <https://doi.org/10.5194/nhess-10-1829-2010>
- Wolle CM, Carvalho CS (1989a) Deslizamentos em encostas na Serra do Mar - Brasil. *Solos e Rochas* 12:27–36
- Wolle MC, Hachich W (1989b) Rain-induced landslides in southeastern Brazil. In: 12th International conference on soil mechanics and geotechnical engineering, Rio de Janeiro Brasil, pp 1639–1642
- Wu W, Sidele RC (1995) A Distributed Slope Stability Model for Steep Forested Basins *Water Resources Research* 31:2097–2110. <https://doi.org/10.1029/95wr01136>